Available online at www.sciencedirect.com
ScienceDirect
Journal of Sound and Vibration 299 (2007) 806–821
JOURNAL OF SOUND AND VIBRATION
www.elsevier.com/locate/jsvi

Influence of stiffness and contact modelling on catenary–pantograph system dynamics

O. Lopez-Garcia[a,*], A. Carnicero[b], J.L. Maroño[a]

[a]Instituto de Investigación Tecnológica, Universidad Pontificia Comillas de Madrid, Santa Cruz de Marcenado, 26, 28015 Madrid, Spain
[b]Mechanical Department, Universidad Pontificia Comillas de Madrid, Alberto Aguilera, 23, 28015 Madrid, Spain

Received 17 October 2005; received in revised form 6 July 2006; accepted 13 July 2006
Available online 2 October 2006

Abstract

This article is concerned with dynamic simulation of catenary–pantograph interaction using simplified models. The paper proposes the improvement of these models by considering an enhanced catenary stiffness model and contact modelling based on lagrangian multipliers. The influence of both enhancements is discussed and investigated by means of an exhaustive comparison between most common simplified models and the method proposed herein. The results show that catenary stiffness modelling plays a central role at low train speed. Contact modelling allows a more accurate description of contact force during contact losses and is the critical factor at high train speeds.

1. Introduction

This article deals with dynamic behaviour of the interaction between railway catenary and train pantograph. The railway catenary or overhead line is made of a complex system of cables that provides the electrical energy supply to the train by means of the contact between the pantograph of the vehicle and the catenary itself. In its simplest form, the catenary consists of three main components. The contact wire supplies the electrical energy to the train, the messenger wire provides sufficient stiffness to the catenary and the droppers link both wires, see Fig. 1. Dynamic behaviour of the catenary–pantograph is reviewed in Ref. [1] by giving an overview of the most important methods used to describe catenary and pantograph system dynamics. From a more general railway perspective and regarding in particular flexible multibody techniques, catenary–pantograph interaction is briefly reviewed in Ref. [2].

Two main groups of dynamic interaction simulation models exist. On one hand, there are authors that use numerical methods to solve the full catenary–pantograph interaction problem. In Ref. [3] the authors use the finite element method (FEM) to model the catenary; a nonlinear lumped parameter system to describe the pantograph; and a penalty method to model contact between catenary and pantograph. The analysis of the catenary–pantograph interaction using multibody computational techniques and Lagrange multipliers has

*Corresponding author. Tel.: +34 91 542 28 00; fax: +34 91 542 31 76.
E-mail addresses: oscar.lopez@iit.upcomillas.es (O. Lopez-Garcia), carnicero@dim.icai.upcomillas.es (A. Carnicero), joseluis.marono@iit.upcomillas.es (J.L. Maroño).

0022-460X/$ - see front matter © 2006 Elsevier Ltd. All rights reserved.
doi:10.1016/j.jsv.2006.07.018

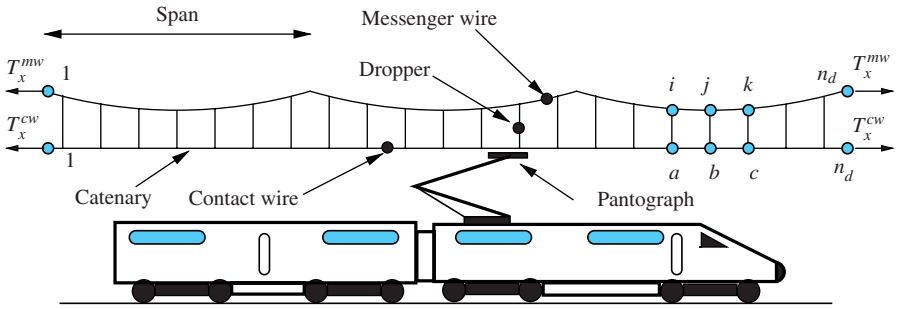

Fig. 1. Catenary and pantograph dynamic interaction.

been recently studied in Ref. [4]. A more mathematical approach using partial differential equations coupled to differential-algebraic equations can be found in Refs. [5–7]. Lumped masses linked to massless bars to model the catenary and a linear lumped parameter system to represent the pantograph were used to study overhead resonance with multi-pantographs in Ref. [8].

The main advantage of these approaches is that simulation results show a better agreement with real data. However, the shortcomings are the high computational cost and the inherent numerical errors. Moreover, due to computer and run time requirements, it would not be feasible to use these techniques to carry out parameter studies, dynamic stability analysis or catenary–pantograph optimization.

In order to overcome these deficiencies, simplified models have been developed. In Ref. [9] the Fourier transform is applied to an infinite string supported by springs separated by the span length, in order to investigate the periodical dynamic stability. In Ref. [10] a linear dynamic model of one degree of freedom (dof) with time varying stiffness coefficient is formulated and using a simplified stiffness function, the system is treated as a Mathieu equation and the dynamic stability is analysed using the Floquet theory. However, regarding stability analysis some deficiencies were encountered and applying Hill's method of infinite determinants in Ref. [11] the actual stability boundaries were presented. Fourier transform using Floquet's theory is applied to a periodically spring-supported string subjected to a moving load in Ref. [12]. Due to its simplified or analytical nature, these models reduce the mathematical and physical complexity of the problem and consequently the computational effort, decreasing the time required to run full simulations. Therefore, these models are well suited for analysing dynamic stability or the influence of catenary and pantograph parameters on the dynamic behaviour of the system. For instance, in Ref. [13], a dynamic sensitivity analysis to choose the appropriate dynamic parameters of the pantograph is carried out using a linear lumped dynamic system together with a simplified catenary stiffness model.

Most of the simplified models propose analytical approximations for the dynamic parameters of the catenary, in order to avoid complicated FE computations from which they are obtained. The catenary stiffness is simplified by fitting cosine functions to FEM results in Refs. [10,13]. Mass, damping and stiffness are fitted to experimental data by superposition of cosine functions in Ref. [14]. Dynamic stiffness computation is based on FEM calculations to determine the stiffness, density and tension catenary parameters in Ref. [12]. However, all these descriptions smoothen the actual mass, damping and stiffness along the span, avoiding one important source of dynamic excitation.

The goals of the paper are to add some improvements to current simplified models and to discuss the effect of these enhancements on dynamic interaction of the catenary–pantograph system. In this paper two contributions are presented. Firstly, the influence of an improved stiffness model in the dynamic behaviour of catenary–pantograph interaction is studied by applying the method published in Ref. [15] to compute the catenary stiffness. The advantages of this method are accuracy, robustness and speed. Secondly, a contact model using Lagrange multipliers is incorporated into the dynamic equations of the catenary–pantograph system and its influence on the overall dynamic response is investigated. Due to the nature of both enhancements, the equations can no longer be treated analytically anymore and numerical tools must be employed to obtain a precise solution. Regarding these aspects, the proposed method must be considered as one that is a mix between both complex and simplified models.

As it is well known, Lagrange multipliers may inadequately model the case of loss of contact which is an important issue in catenary–pantograph interaction. In Ref. [4] this problem is addressed by proposing a penalty formulation that produces a unilateral force in order to substitute the interpenetrability constraint. However, the problem remains open in the sense that this solution is only proposed and not studied. In the method proposed here, the loss of contact and subsequent possible contact recovery is treated as a natural consequence of the proposed formulation.

Another common assumption of simplified models is neglecting wave propagation, see for instance Refs. [10,14]. One major exception is the dynamic catenary stiffness calculation presented in Ref. [12], which takes into account wave propagation. However, recent papers using simplified models, i.e. [13] have carried out dynamic sensitivity analysis without considering wave propagation in an attempt to find a tradeoff between complexity and performance. In order to highlight the influence of the proposed enhancements, wave propagation will be neglected in this paper.

The remainder of the paper is organized as follows. Section 2 describes the foundations of the method. The goals of this section are twofold. On one hand, the proposed stiffness computation is reviewed and implemented in the dynamic equations of the motion. On the other hand, contact modelling by means of lagrangian multipliers is incorporated into the differential ordinary equations of the motion. Section 3 provides the application of the aforedescribed method to simulate catenary–pantograph interaction and the comparison with more simplified models. Finally, in Section 4, the main conclusions of this study are drawn.

2. Theoretical foundations of the method

In this section the method used to compute catenary stiffness is presented and the equations of motion of the proposed simplified catenary–pantograph lumped model, including contact modelling, are derived.

2.1. Catenary stiffness computation

Let us consider a catenary overhead made of two main wires, called contact and messenger wires, connected by a finite number of droppers, n_d. Properties related to contact and messenger wires will be denoted by cw and mw superscripts, respectively. Fig. 1 shows a sketch of the overall system. The connection points between droppers, contact and messenger wires will be referred to as nodes. In what follows, the nodes corresponding to messenger and contact wire will be denoted by $j = 1 \ldots n_d$ and $b = 1 \ldots n_d$, respectively, and the dropper which connects node j with node b will be referred to as dropper q. Horizontal and vertical vector components will be denoted by subindexes x and y, respectively. The mass per unit length of droppers, messenger and contact wires is denoted by λ^q, $\lambda^{\mathrm{mw}}$and λ^{cw}. Railway overheads are subjected to messenger and contact wire tensions, T^{mw} and T^{cw}, respectively, which are applied at the catenary boundary supports as shown in Fig. 1.

Applying force equilibrium at messenger wire node j, contact wire node b, and dropper q, see Fig. 2, the following set of equations are obtained:

$$\mathbf{T}^{j^+} + \mathbf{T}^{j^-} + \mathbf{R}^j + m^j\mathbf{g} = \mathbf{0}, \tag{1}$$

$$\mathbf{T}^{b^+} + \mathbf{T}^{b^-} + \mathbf{R}^b + m^b\mathbf{g} + \mu = \mathbf{0}, \tag{2}$$

$$\mathbf{R}^j + \lambda^q s^q \mathbf{g} + \mathbf{R}^b = \mathbf{0}, \tag{3}$$

where index j and b refer to messenger and contact wire nodes, superindex $+$ applies to the right side of the node and $-$ to the left side of the node . The tension vector is denoted by $\mathbf{T}$, node reaction is $\mathbf{R}$, m^j and m^b are the messenger and contact suspension clamp masses, respectively, s^q is the distance between contact and messenger wire nodes, $\mathbf{g}$ is the gravity acceleration vector and μ is the force acting on the contact wire due to the interaction between catenary and pantograph.

The horizontal component of Eqs. (1) and (2), states that the horizontal components of cable tensions must be equal. Taking into account the fact that the tension can be written in terms of the horizontal components,

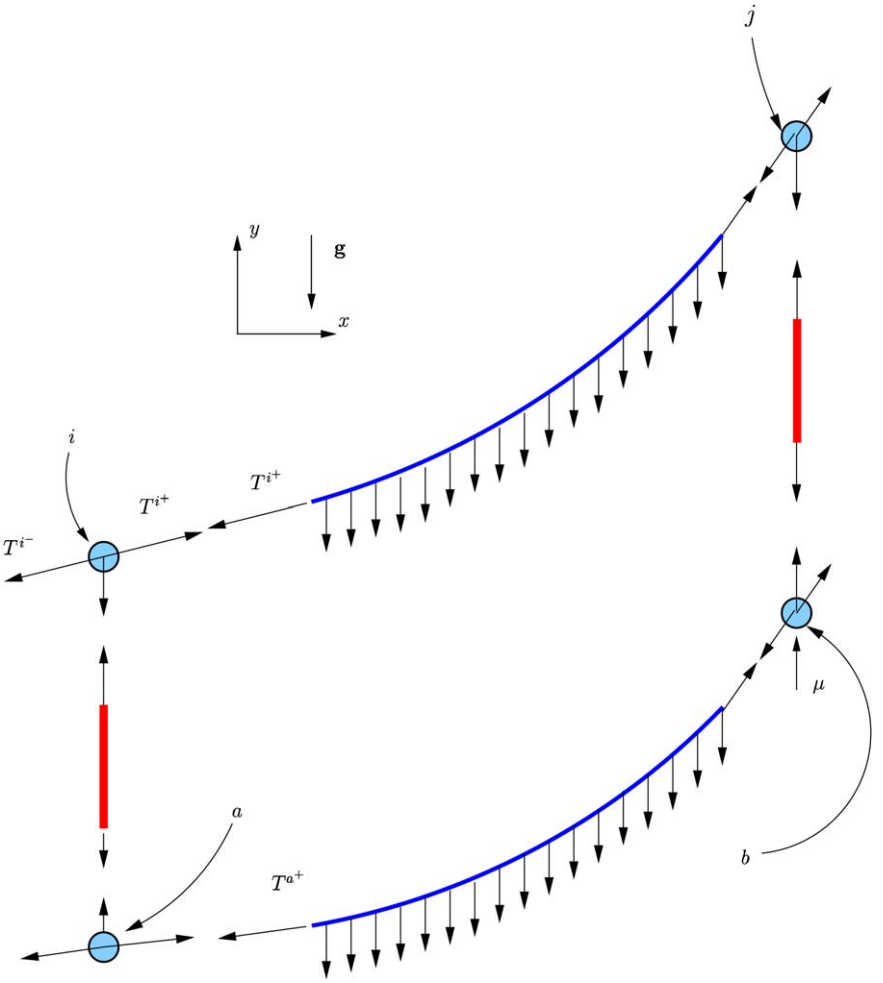

Fig. 2. Droppers, messenger and contact wires force analysis.

the following expression is obtained:

$$\mathbf{h(t)} = \mathbf{0}, \tag{4}$$

where $\mathbf{t} = (T_x^{\mathrm{mw}}, T_x^{\mathrm{cw}})$ is the horizontal tension vector and $\mathbf{h} = (h^{\mathrm{mw}}, h^{\mathrm{cw}})$ can be expressed by

$$h^{\mathrm{mw}} = T_x^{\mathrm{mw}} \cosh\left(\alpha^{ij} + \frac{x^j - x^i}{2C^{\mathrm{mw}}}\right) - T^{\mathrm{mw}}, \qquad i = 1, \quad j = 2, \tag{5}$$

$$h^{\mathrm{cw}} = T_x^{\mathrm{cw}} \cosh\left(\alpha^{ab} + \frac{x^b - x^a}{2C^{\mathrm{cw}}}\right) - T^{\mathrm{cw}}, \qquad a = 1, \quad b = 2, \tag{6}$$

where C is the catenary characteristic length $C = T/\lambda g$ and α is defined by

$$\alpha(x^-, y^-, x^+, y^+, \lambda g, T_x) = \mathrm{Asinh}\left(\frac{y^+ - y^-}{2C \sinh\left(\dfrac{x^+ - x^-}{2C}\right)}\right), \tag{7}$$

where Asinh $(\bullet)$ stands for the inverse hyperbolic sine of $\bullet$.

Expressing the vertical component of tensions as functions of the catenary position, using the force equilibrium at dropper, and canceling the reactions, the whole system of equations can be rewritten as

$$\mathbf{f}(\mathbf{y}^j, \mathbf{y}^b, \mathbf{t}; \mu) = \mathbf{0}, \tag{8}$$

where $\mathbf{y}^j = (y^1, \ldots, y^j, \ldots, y^{n_d})$, $\mathbf{y}^b = (y^1, \ldots, y^b, \ldots, y^{n_d})$ and $\mathbf{f} = (f^1, \ldots, f^q, \ldots, f^{n_d})$. The function f^q represents the vertical equilibrium of forces in terms of the vertical position of contact and messenger wire nodes, y^b and y^j, respectively, and is defined by

$$\begin{aligned} f^q(y^j, y^b) = {} & T_x^{\mathrm{mw}} \sinh\left(\alpha^{jk} + \frac{x^k - x^j}{2C^{\mathrm{mw}}}\right) - T_x^{\mathrm{mw}} \sinh\left(\alpha^{ij} + \frac{x^i - x^j}{2C^{\mathrm{mw}}}\right) \\ & + T_x^{\mathrm{cw}} \sinh\left(\alpha^{ab} + \frac{x^a - x^b}{2C^{\mathrm{cw}}}\right) - T_x^{\mathrm{cw}} \sinh\left(\alpha^{bc} + \frac{x^c - x^b}{2C^{\mathrm{cw}}}\right) \\ & - g(m + \lambda^q s^q) + \mu, \end{aligned}$$

where $m = m^j + m^b$ is the total clamp mass of the dropper.

The catenary stiffness must be computed using an algorithm that firstly obtains the dropper length, that is, computing the initial equilibrium configuration of the catenary due to its own weight and finally determining the deformed configuration caused by the force exerted on the contact wire as consequence of the pantograph interaction. In Table 1 the computation scheme is shown. A two nested Newton–Raphson procedure is applied to solve the problem where Jacobian matrices are denoted by $\mathbf{H} = \partial\mathbf{h}/\partial\mathbf{y}$ and $\mathbf{F} = \partial\mathbf{f}/\partial\mathbf{y}$. More information on the method details and validation computations can be found in Ref. [15].

2.1.1. Initial equilibrium configuration

Determining the initial equilibrium configuration of the catenary involves finding the messenger wire position which satisfies the constraint of an imposed contact wire position $\varphi^b = \varphi(\mathbf{y}^b)$ given geometry properties, tension of contact and messenger wires, mass properties of droppers and clamps, and density of contact and messenger wires. The solution of this problem is obtained using the first part of Table 1 where $\mathbf{A}(\mathbf{y}^j) = \mathbf{F}(\mathbf{y}^y; \varphi^b, \mathbf{t}, 0)$. Then, the dropper length can be easily computed as $l^q = y^j - \varphi^b$.

Table 1
Stiffness computation algorithm

(1) Compute initial equilibrium configuration under $\mu = 0$
- Constraints: $\varphi(\mathbf{y}^b) = 0$
- *while* $\mathbf{h}(\mathbf{t}_{n+1}) > \mathtt{TOL}$
  - $\mathbf{t}_n = \mathbf{t}_{n+1}$
  - $\mathbf{t}_{n+1} = \mathbf{t}_n - (\mathbf{H}(\mathbf{t}_n))^{-1} \cdot \mathbf{h}(\mathbf{t}_n)$
  - *while* $\mathbf{f}(\mathbf{y}^j_{n+1}) > \mathtt{TOL}$
    - $\mathbf{y}^j_n = \mathbf{y}^j_{n+1}$
    - $\mathbf{y}^j_{n+1} = \mathbf{y}^j_n - (\mathbf{A}(\mathbf{y}^j_n))^{-1} \cdot \mathbf{f}(\mathbf{y}^j_n)$
  - *end*
- *end*

(2) Compute deformed configuration under μ
- Constraint: $\Lambda(\mathbf{y}^j; \mathbf{l}^q) = 0$
- *while* $\mathbf{h}(\mathbf{t}_{n+1}) > \mathtt{TOL}$
  - $\mathbf{t}_n = \mathbf{t}_{n+1}$
  - $\mathbf{t}_{n+1} = \mathbf{t}_n - (\mathbf{H}(\mathbf{t}_n))^{-1} \cdot \mathbf{h}(\mathbf{t}_n)$
  - *while* $\mathbf{f}(\mathbf{y}^b_{n+1}) > \mathtt{TOL}$
    - $\mathbf{y}^b_n = \mathbf{y}^b_{n+1}$
    - $\mathbf{y}^b_{n+1} = \mathbf{y}^b_n - (\mathbf{B}(\mathbf{y}^b_n))^{-1} \cdot \mathbf{f}(\mathbf{y}^b_n)$
  - *end*
- *end*

2.1.2. Deformed configuration

Once initial catenary configuration (i.e. dropper lengths) is determined, the stiffness function along several spans can be computed. The stiffness can be regarded as the relationship between a given vertical force, μ, acting on a determined position of the contact wire, and the vertical displacement of this point. Therefore, vertical coordinates of the messenger wire nodes can be expressed as functions of the unknowns as $y^j = l^q + y^b$ where the length of every dropper has been previously computed and therefore provide the equation $\Lambda^j = \Lambda(\mathbf{y}^j; \mathbf{l}^q)$. Vertical displacements of the contact wire can be computed by means of the second part of Table 1 where $\mathbf{B}(\mathbf{y}^b) = \mathbf{F}(\mathbf{y}^b; \Lambda^j, \mathbf{t}, \mu)$. Once the vertical displacements of the contact wire are found, the catenary stiffness at position x^c can be obtained as

$$k_c(x^c) = \frac{\mu}{y^c},$$

where y^c is the vertical displacement of the contact wire at position x^c.

2.2. Dynamic equations of motion

In this subsection a simplified model of the catenary–pantograph interaction is provided. The catenary is described by equivalent mass, damping and stiffness of a 1 dof system. The pantograph is considered a 2 dof lumped system. This description of the pantograph dynamics is one of the most widely used, see for instance Refs. [8,10]. Let us consider the generalized coordinates $\mathbf{y} = \{y_c, y_1, y_2\}$ that represents the vertical displacements of the catenary–pantograph equivalent system shown in Fig. 3. Subscripts $c, 1, 2$ stand for catenary, pantograph head and pantograph base, respectively. In this kind of simplified model, it is usually assumed that the pantograph head is always connected to the catenary contact wire, and furthermore, the contact force is computed as the catenary stiffness multiplied by the catenary vertical displacement, see Refs. [13,12]. One of the contributions of this paper is to add a more realistic description of the contact process between catenary and pantograph, by modelling it appropriately.

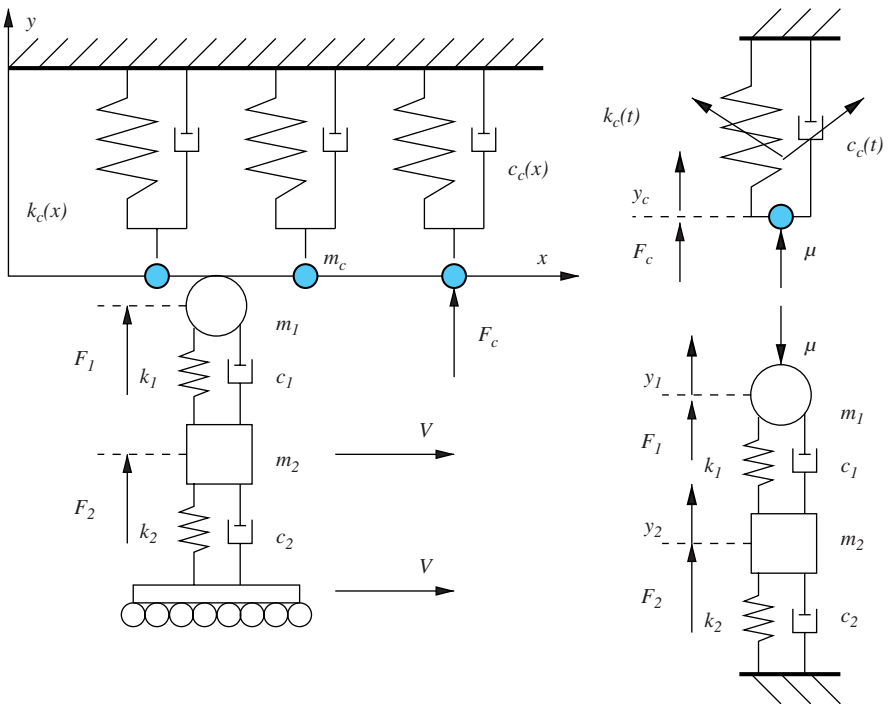

Fig. 3. Catenary overhead and pantograph equivalent model.

The interaction between catenary and pantograph can be modelled in several different ways. The most common approach consists of coupling dynamical equations of catenary and pantograph, by providing equations that connect state variables of both systems. Despite the fact that controversy exists regarding penalty methods and elastic elements to describe contact wire (as pointed out in Ref. [1]), a two-parameter contact penalty model has been implemented, checked and applied in Ref. [3] with good results. Penalty methods are easily implemented, especially using FEM. However, one important drawback of this method is the selection process used to define the parameters of the method. In this paper a lagrangian contact model is proposed to model the interaction between catenary and pantograph. As contact is point-to-point, Lagrange contact method can be easily implemented, and the problem of selecting parameters to set up the calculations is ignored. A more general three-dimensional framework of the Lagrange contact method and its application to the catenary–pantograph interaction can be found in Ref. [4]. In this reference, a sliding joint constraints the relative motion between catenary and pantograph in a plane perpendicular to the catenary centreline. Another difference is that the method proposed herein uses a contact condition based only on displacements and the aforecited reference constraints not only position but also velocity and acceleration. Moreover, and as will be seen below, the Lagrange multiplier of the proposed contact model has a very clear physical interpretation.

In order to include the contact forces, a condition where there is no penetration between catenary and pantograph head must be imposed, that is $Y(\mathbf{y}) = y_1 - y_c \leqslant 0$. In order to fulfil this inequality a constrained lagrangian, $L(\mathbf{q}, \dot{\mathbf{q}})$, is defined by

$$L(\mathbf{q}, \dot{\mathbf{q}}) = T(\dot{\mathbf{y}}) - V(\mathbf{y}) - \mu Y(\mathbf{y}),$$

where $\mathbf{q} = \{y_c, y_1, y_2, \mu\}$ are the generalized coordinates of the constrained problem, $T(\dot{\mathbf{y}})$ is the kinetic energy, $V(\mathbf{y})$ the work done by conservative forces, and μ is the Lagrange multiplier which in this context plays the very clear role of contact force. The term $\mu Y(\mathbf{y})$ can be regarded as the work done by contact forces. The kinetic and potential functions are expressed by

$$T(\dot{\mathbf{y}}) = \tfrac{1}{2} m_c \dot{y}_c^2 + \tfrac{1}{2} m_1 \dot{y}_1^2 + \tfrac{1}{2} m_2 \dot{y}_2^2,$$
$$V(\mathbf{y}) = \tfrac{1}{2} k_c y_c^2 + \tfrac{1}{2} k_1 (y_1 - y_2)^2 + \tfrac{1}{2} k_2 y_2^2,$$

where the symbols m, and k stand for mass, and stiffness, respectively. The nonconservative forces are viscous forces with damping parameter c, which are described by the Rayleigh dissipation function

$$D(\dot{\mathbf{y}}) = \tfrac{1}{2} c_c \dot{y}_c^2 + \tfrac{1}{2} c_1 (\dot{y}_1 - \dot{y}_2)^2 + \tfrac{1}{2} c_2 \dot{y}_2^2$$

and the external generalized forces are $\mathbf{Q} = \{F_c, F_1, F_2, 0\}$, which are the aerodynamic lift forces at catenary, pantograph head and the external force applied to the pantograph base, respectively.

Finally, the dynamic equations of the equivalent catenary–pantograph system are obtained using the Lagrange equation

$$\frac{\mathrm{d}}{\mathrm{d}t}\left(\frac{\partial L}{\partial \dot{\mathbf{q}}}\right) - \frac{\partial L}{\partial \mathbf{q}} + \frac{\partial D}{\partial \dot{\mathbf{q}}} = \mathbf{Q}$$

which leads to the following differential algebraic equation system with time-varying coefficients:

$$\left[\begin{array}{c|c} \mathbf{M} & \mathbf{0} \\ \hline \mathbf{0} & 0 \end{array}\right] \cdot \left\{\begin{array}{c} \ddot{\mathbf{y}} \\ \hline \ddot{\mu} \end{array}\right\} + \left[\begin{array}{c|c} \mathbf{C} & \mathbf{0} \\ \hline \mathbf{0} & 0 \end{array}\right] \cdot \left\{\begin{array}{c} \dot{\mathbf{y}} \\ \hline \dot{\mu} \end{array}\right\} + \left[\begin{array}{c|c} \mathbf{K}(t) & \mathbf{G}^{\mathrm{T}} \\ \hline \mathbf{G} & 0 \end{array}\right] \cdot \left\{\begin{array}{c} \mathbf{y} \\ \hline \mu \end{array}\right\} = \left\{\begin{array}{c} \mathbf{F} \\ \hline 0 \end{array}\right\}, \quad \leq \tag{9}$$

where superscript T stands for transpose, $\mathbf{M}, \mathbf{C}$, and $\mathbf{K}$ are the mass, damping and stiffness matrices, respectively, and can be expressed by

$$\mathbf{M} := \begin{bmatrix} m_c & 0 & 0 \\ 0 & m_1 & 0 \\ 0 & 0 & m_2 \end{bmatrix}, \quad \mathbf{C} := \begin{bmatrix} c_c & 0 & 0 \\ 0 & c_1 & -c_1 \\ 0 & -c_1 & c_1 + c_2 \end{bmatrix}, \quad \mathbf{K} := \begin{bmatrix} k_c(t) & 0 & 0 \\ 0 & k_1 & -k_1 \\ 0 & -k_1 & k_2 + k_1 \end{bmatrix},$$

where

$$\mathbf{G} = [-1, \quad 1, \quad 0] \quad \text{and} \quad \mathbf{F} = [F_c, \quad F_1, \quad F_2]$$

is the external applied force vector.

It must be remarked that the mass of the catenary overhead is usually neglected with respect to the other inertia contributions, see for instance Refs. [13,8,10]. The goal of this paper is to study the influence of contact forces and catenary stiffness modelling, so in order to obtain a clearer picture of the effect of both aspects, catenary mass and damping, and aerodynamic forces are disregarded in the numerical simulations.

From the inequality of the penetration constraint, Kuhn–Tucker conditions are applied to compute contact force. If contact is present, due to the impenetrability condition $Y(\mathbf{y})$, then $y_1 = y_c$, the contact force is positive, $\mu > 0$ and is obtained together with $\mathbf{y}$ from the integration of Eq. (9). If there is no contact between catenary and pantograph, $y_1 - y_c \leqslant 0$ then $\mu = 0$, that is, the contact force is zero and $\mathbf{y}$ is calculated from the integration of Eq. (9).

3. Numerical simulation results

In the following, the results of the numerical simulations that have been carried out are presented and discussed. The system of differential equations (9) has been solved by means of a fourth-order Runge–Kutta method taking into account Kuhn–Tucker conditions.

The catenary and pantograph that are used to carry out the simulations are defined by Manabe and Fujii in Ref. [8]. The catenary corresponds to the simple catenary presented in this reference and the pantograph parameters are: $m_1 = 6.5\,\text{kg}$, $c_1 = 120\,\text{Ns/m}$, $k_1 = 39\,\text{kN/m}$, $m_2 = 8.5\,\text{kg}$, $c_2 = 30\,\text{Ns/m}$, $k_2 = 0$ and $F_2 = 54\,\text{N}$. These values correspond to the information provided by the aforementioned reference.

In Fig. 4 the stiffness variation along the span of the simple catenary defined by Manabe and Fujii [8] is shown. In this figure two functions are represented: stiffness computed using the aforementioned method, nonsmooth stiffness, and the smooth stiffness widely used by simplified dynamic models. The smooth stiffness is calculated from the maximum, $k_{\max}$, and minimum, $k_{\min}$, values of stiffness by means of the function proposed in Ref. [10] as

$$k(x) = \frac{k_{\max} + k_{\min}}{2}\left[1 + \frac{k_{\max} - k_{\min}}{k_{\max} + k_{\min}}\cos\left(\frac{2\pi x}{L}\right)\right]. \tag{10}$$

Two main differences can be found between them. The first one refers to the variability of the nonsmooth stiffness, showing a more irregular pattern due to presence of the droppers which locally increments the stiffness with respect to the smooth one. The second one is the important difference in value through the whole catenary span, between smooth and nonsmooth stiffness functions. In fact, the ratio between mean smooth stiffness and mean nonsmooth stiffness is about 1.2. Furthermore, at localized points smooth stiffness values can be about two times nonsmooth stiffness values. As it will be seen later these two differences play an important role in the type of obtained simulation results. It should be remarked that several authors used the type of approximation shown in Eq. (10) but Refs. [12] or [13], for reasons unknown, fail to properly relate stiffness approximation to computed stiffness results.

In order to understand how the simulation results are influenced by contact and catenary stiffness modelling, the following models have been considered.

- SSNC stands for smooth stiffness and noncontact model. This formulation does not incorporate a contact model and pantograph head, and catenary are always supposed to be in contact. Moreover, it will provide a

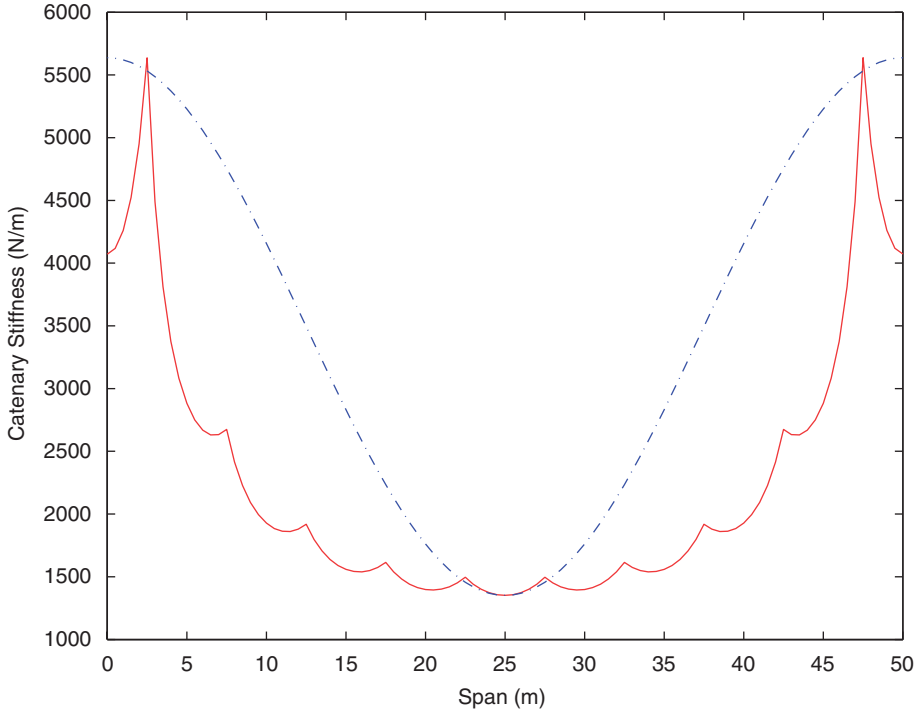

Fig. 4. Stiffness comparison between nonsmooth stiffness (—) and smooth stiffness (–·–).

basis for comparison purposes because it represents the simplest approach and it is also the most commonly used.

- SSWC refers to a smooth stiffness with contact model. The results of this model take into account a smooth description of the catenary stiffness but uses a lagrangian contact formulation to appropriately describe the contact between pantograph overhead and catenary. Therefore, contact losses can be properly taken into account.
- NSNC refers to a nonsmooth stiffness with noncontact model. In fact, this model uses a nonsmooth stiffness function and considers catenary and pantograph overhead to be in contact at all times, and consequently cannot be considered that proper contact loss is taken into account.
- NSWC stands for nonsmooth stiffness with contact model. Finally, this model fully exploits the benefits of the method proposed herein by taking into account not only the nonsmooth catenary stiffness but also proper contact modelling.

The equation of motion for every model can be easily derived from the more general case of Eq. (9).

Two main results are discussed. Firstly, maximum and peak-to-peak contact forces as a function of operational train speed have been obtained. In this way, contact losses can be found when the peak-to-peak contact force is greater than the maximum contact force. Secondly, and specifically, contact force time series are represented for every model at two representative operational train speeds.

In Figs. 5 and 6 the comparison between SSWC and SSNC models is shown. This comparison determines the influence of the contact model when smooth stiffness is used in the simulations. As was previously pointed out in Ref. [10], the maximum contact force dependence on train speed when the SSNC model is used exhibits three maxima for values of the ratio between frequency of span travelled and eigenfrequency of catenary–pantograph system closer to $1, \frac{1}{2}$, and $\frac{1}{3}$. For the SSNC model, the contact force exhibits a maximum at ratios which correspond to velocities of approximately 410, 210 and 140 km/h, and shows a good agreement with the theoretical values obtained in Refs. [10,12]. However, the SSWC model shows a smoother variation of contact force with velocity, two maxima points about 140 and 270 km/h, and a quite different tendency at train speeds higher than 250 km/h. Both models predict contact loss at train speeds higher than 130 km/h. The

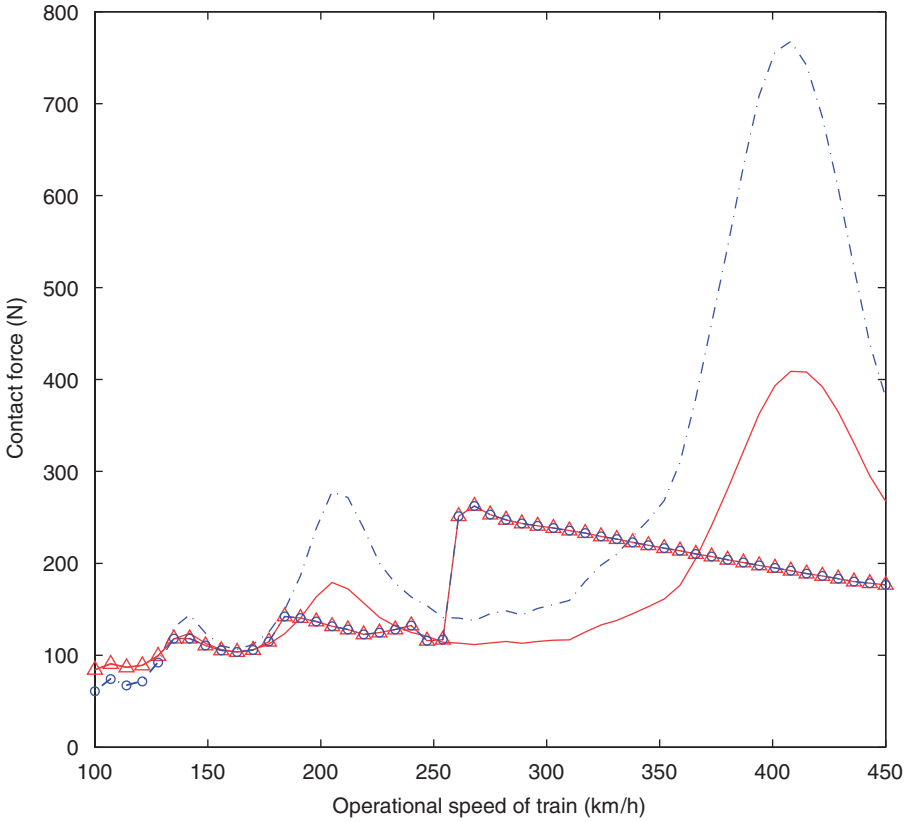

Fig. 5. Comparison of contact force dependency on operational train speed between SSWC maximum contact force (△–△), SSWC peak-to-peak force (○–·–○), SSNC maximum contact force (—), SSNC peak-to-peak force (–·–).

contact force response of the SSWC model at low train speeds is similar to the SSNC model but differs at the train speed range in which contact losses are computed (from 130 km/h onwards). As SSWC includes the proper contact modelling, maximum and peak-to-peak contact forces must be equal during contact losses. One major weakness of the SSNC model is that when contact losses appear, the contact forces are incorrectly computed due to the assumption that catenary and pantograph are always in contact. This aspect implies that peak-to-peak forces are higher and that the contact force is amplified due to inertia effects. In Fig. 6, contact force time series are depicted and differences when comparing contact or noncontact models are quite considerable. Both of them present smooth time variation as both models share smooth stiffness approximation. However, the SSNC model exhibits negative contact forces which are obviously impossible. Conversely, SSWC shows a nonsmooth contact force time variation due to the fact that when contact loss appear the contact force is zero. Therefore, the difference between SSWC and SSNC models at train speeds higher than 180 km/h can be explained as a result of the contact loss in this range of velocities and the addition of a contact model which becomes more important at high velocities.

In Figs. 7 and 8, SSNC and NSNC models are compared. These figures illustrate how nonsmooth stiffness influences the computation results. Contrary to the SSWC, the main difference with respect to the reference model occurs at low train speeds. The NSNC model predicts contact loss at train speeds higher than 260 km/h and contact force response shows three maxima at velocities of 360, 170 and 115 km/h. Therefore, there exists a velocity shift regarding train speeds at which maxima contact force is attained. This response shift mainly corresponds to the difference between mean nonsmooth to smooth stiffness values. In fact, they are shifted approximately by a factor of the square root of the mean nonsmooth and smooth stiffness ratio. Contact forces computed using NSNC are lower at low speeds than the ones predicted by SSNC because nonsmooth stiffness is lower than smooth stiffness, and both models compute contact force as catenary stiffness multiplied by the pantograph head displacement. However, nonsmooth stiffness variability plays a key role at high speeds and it is responsible for

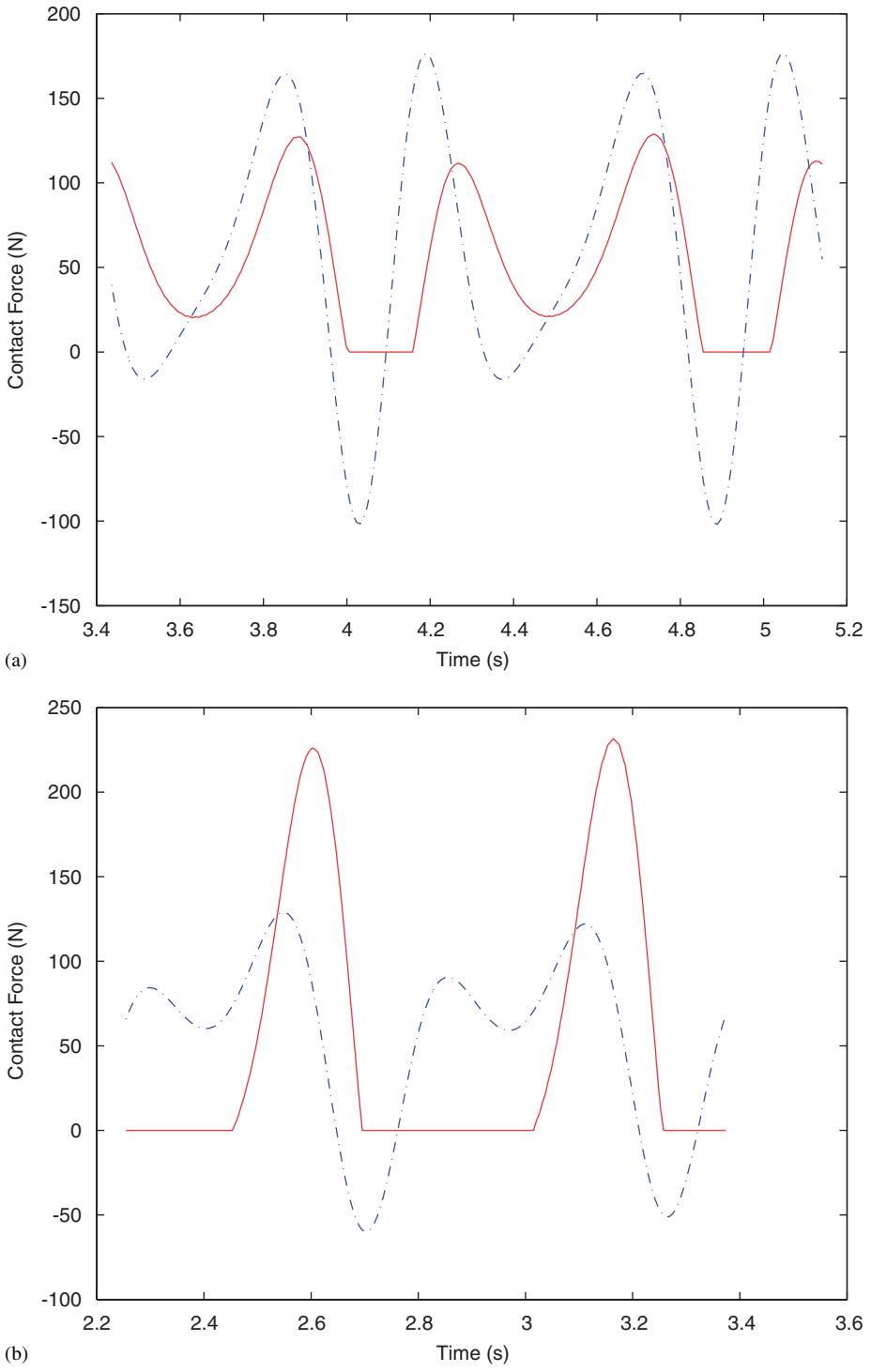

Fig. 6. Comparison between contact force time series computed using SSWC (—) and SSNC (–·–) models (a) $V = 210\,\mathrm{km/h}$ (b) $V = 320\,\mathrm{km/h}$.

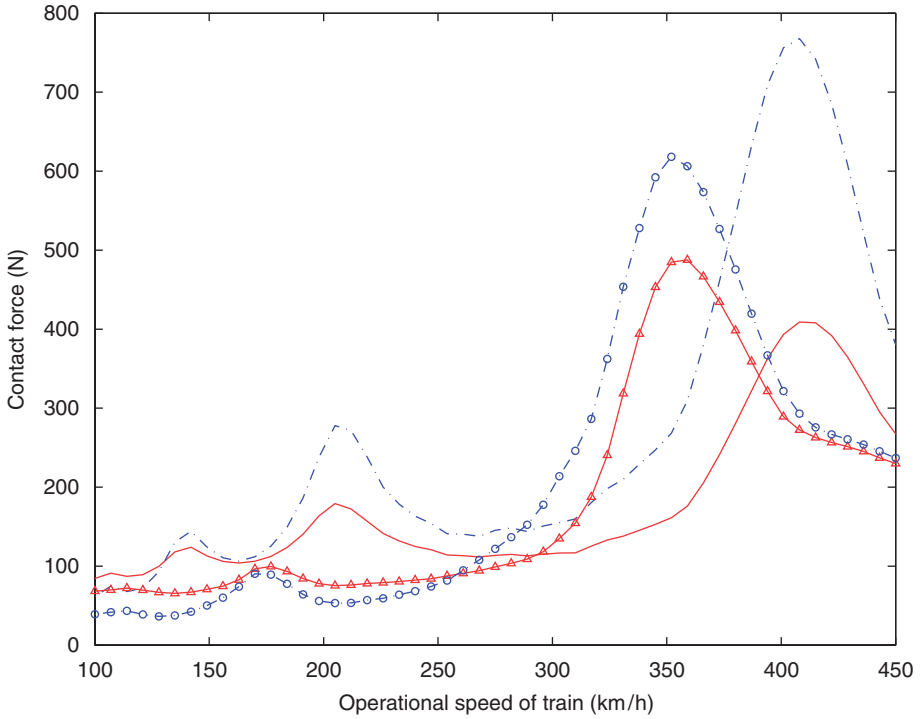

Fig. 7. Comparison of contact force dependency on operational train speed between NSNC maximum contact force (△—△), NSNC peak-to-peak force (○–·–○), SSNC maximum contact force (—), SSNC peak-to-peak force (–·–).

higher contact forces in the vicinity of the maximum than those forces computed using smooth stiffness. Fig. 8 shows contact force time series for both models. When nonsmooth stiffness is considered, contact force time series exhibit a dramatic change. Contact force time evolution does not show a smooth time variation due to local increments of stiffness at the dropper connection which provides a nonregular distribution of stiffness. It can be seen that this local variation is responsible for local increments in the contact force, which can eventually produce contact forces higher than those obtained using smooth stiffness.

NSWC and SSNC models are compared in Figs. 9 and 10. The behaviour of the NSWC model is completely different from the SSNC model, and inherits the two main differences shown by the aforementioned comparisons. Contact loss appears at train speeds higher than 270 km/h. At low train speeds, nonsmooth stiffness computes low contact forces due to lower mean stiffness. At high train speeds, variability of nonsmooth stiffness and contact modelling predicts a more regular variation of contact force dependency on velocity. In fact nonsmooth stiffness variability increases the contact forces in the train speed range from 270 to 450 km/h when these are compared to SSWC model results, raising the maximum contact force from 280 to 350 N. In Fig. 10, contact force time series show a more irregular pattern because two sources of variability are now considered. Firstly, contact forces are always positive, there exists contact between catenary and pantograp, or zero when there is contact loss. And secondly, the local variability of nonsmooth catenary stiffness is also considered.

Summing up, it is clear that taking into account nonsmooth stiffness together with proper contact modelling change dramatically contact force values when they are compared to values obtained using simplified models. Broadly speaking, it can be stated that nonsmooth stiffness plays a key role at low train speeds, whereas the contact model and stiffness variability are more important at high train speeds. Moreover, contact modelling is key to a precise computation of contact wire wear phenomena, not only during catenary–pantograph contact when friction processes govern contact wire wear but also at contact losses, where a reliable calculation of mean displacement gaps is required to compute electric arc wear. Therefore, these two factors are fundamental to understanding the dynamic behaviour of the interaction between catenary and pantograph, and more significantly, most of the simplified models fail to incorporate them into their computations.

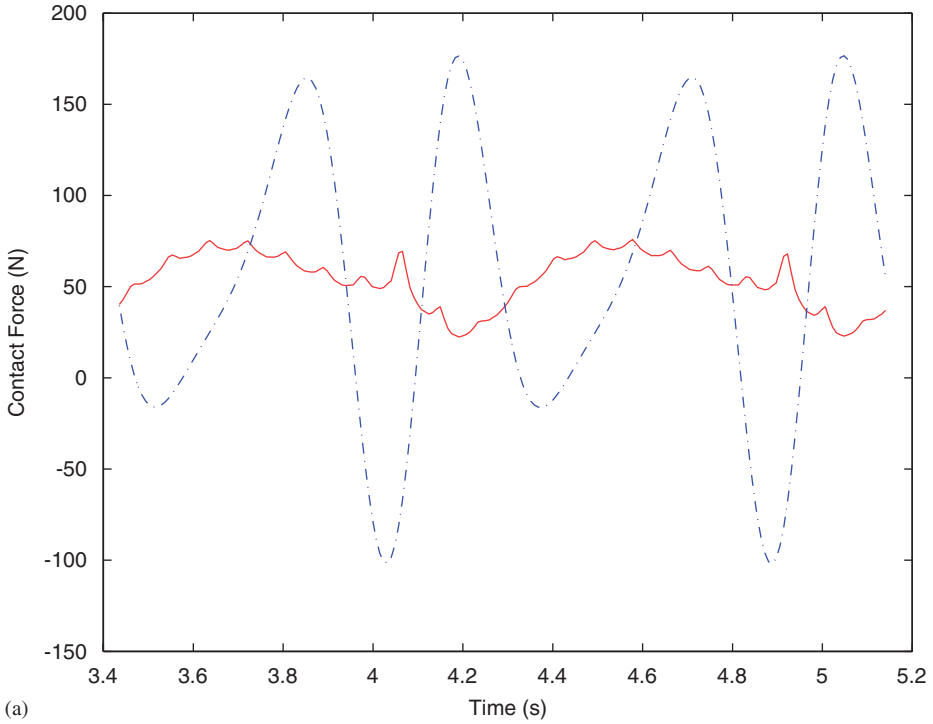

(a)

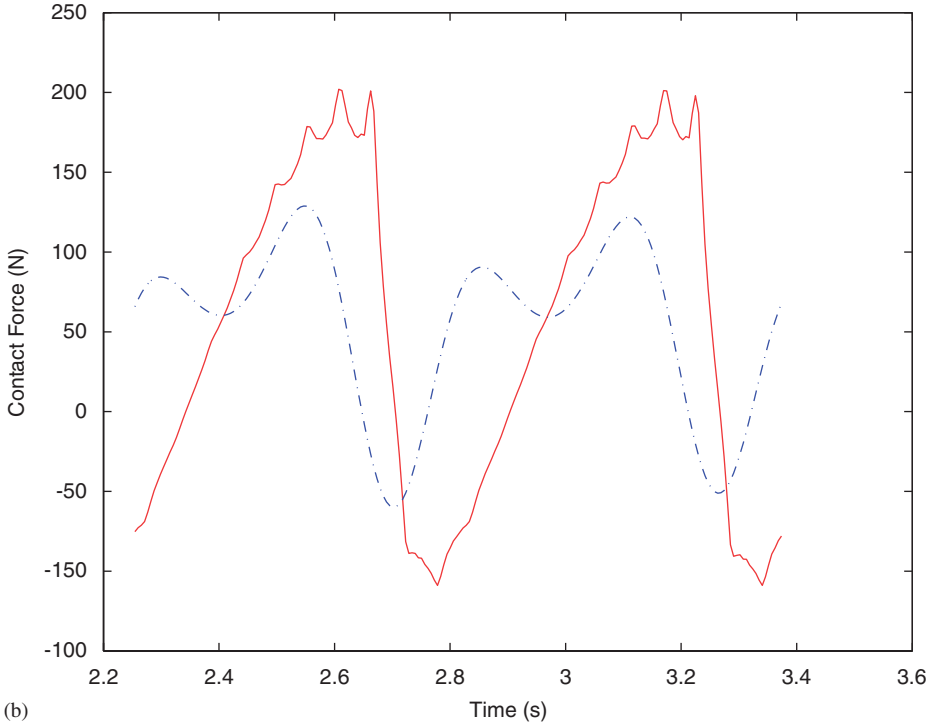

(b)

Fig. 8. Comparison between contact force time series computed using NSNC (—) and SSNC (–·–) models (a) $V = 210\,\mathrm{km/h}$ (b) $V = 320\,\mathrm{km/h}$.

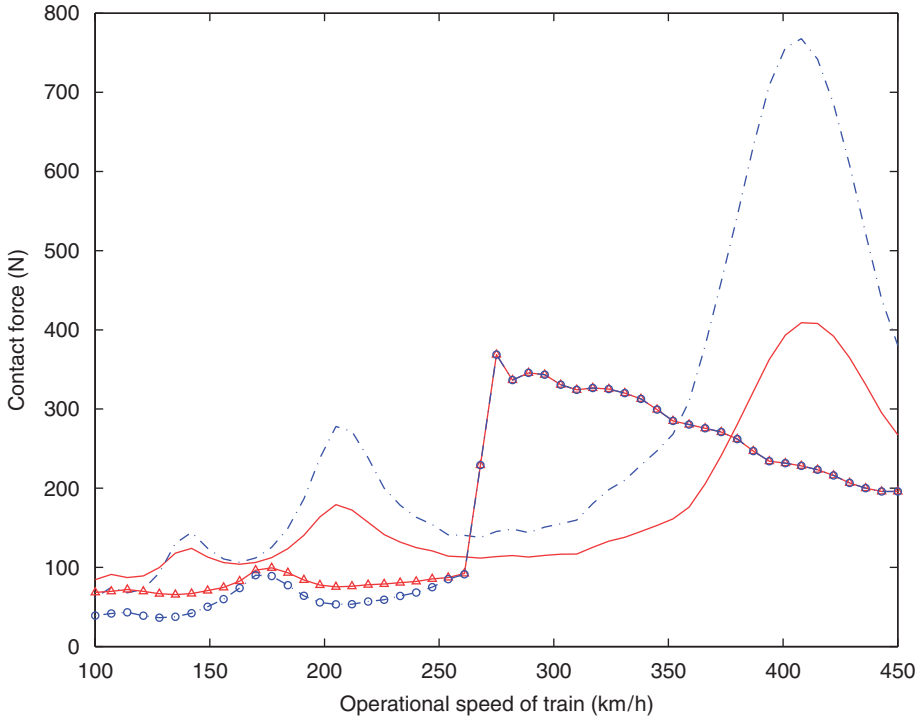

Fig. 9. Comparison of contact force dependency on operational train speed between NSWC maximum contact force (△—△), NSWC peak-to-peak force (○–·–○), SSNC maximum contact force (—), SSNC peak-to-peak force (–·–).

The authors are strongly convinced that these two improvements must be integrated into simplified formulations in order to fully understand actual catenary–pantograph dynamic behaviour. It is important to remark that the computational cost increment is not too high as it may seem at first sight. Despite the fact that complexity of the problem increases, the fast catenary stiffness computation presented allows full simulations to be run in a matter of minutes, thus the proposed method may be used to study parameter variations or catenary–pantograph dynamic optimization in a more efficient way.

4. Conclusions

Many authors have avoided the use of the nonsmooth catenary stiffness function, and due to high computational costs, have developed simplified stiffness descriptions in order to be used in dynamic simulations. One of the contributions of this paper has been to investigate how catenary stiffness computation affects the dynamic simulation of catenary–pantograph interaction. In order to achieve this, a robust and accurate method to quickly compute the nonsmooth catenary stiffness function has been applied, which has been useful in understanding that nonsmooth catenary stiffness plays a major role in predicting contact force evolution. In fact, it has been found that predicted contact losses, when a simplified description of stiffness is used, are not observed when the nonsmooth stiffness is used together with a contact model. Moreover, at low train speeds, dynamic behaviour is highly influenced by the nonsmooth catenary stiffness while nonsmooth stiffness variability increments contact forces particularly at high train speeds.

In this paper the influence of the contact force on the modelling of catenary–pantograph dynamic interaction has been implemented and discussed. The inclusion of a contact model in simplified catenary–pantograph dynamic models allows the correct treatment of the contact loss between catenary and pantograph. The obtained results have shown that the addition of contact modelling to a simplified dynamic model enhances the dynamic response at train speeds in which contact losses appear. Moreover, it has been proven that the influence of contact modelling increases dramatically as train speeds increase. At high

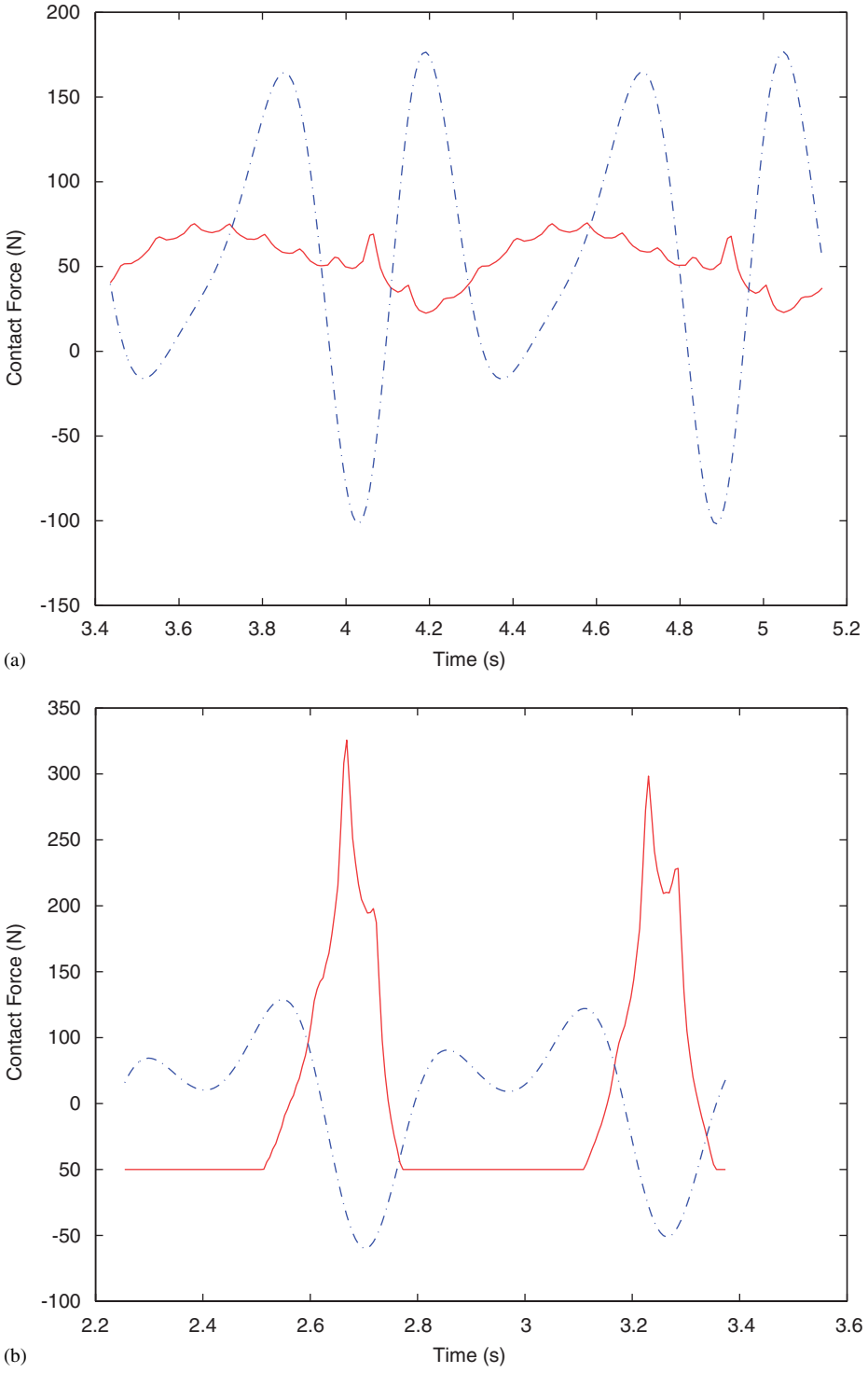

Fig. 10. Comparison between contact force time series computed using NSWC (—) and SSNC (–·–) models (a) $V = 210\,\mathrm{km/h}$ (b) $V = 320\,\mathrm{km/h}$.

train speeds contact modelling plays a central role in understanding the dynamic behaviour of catenary–pantograph interaction.

Due to the simplicity of the proposed model, i.e. point-to-point contact and one dimensional geometry, loss of contact can be well predicted. However, Lagrange contact models can be somewhat not well suited to study loss of contact in a more general geometry frameworks. In order to tackle loss of contact, the authors are currently working on the extension of the Lagrange contact model to consider point-to-segment contact together with perturbed lagrangian techniques.

Despite the fact that the enhancement presented herein clearly improves the results with respect to the most common simplified models, wave propagation is neglected and this must be addressed in the proposed method. To improve this aspect, the authors are working on the dynamic equilibrium equations of the railway catenary, along the lines described in Section 2.1, in order to obtain an nonsmooth dynamic stiffness of the catenary.

Finally a few words about dropper slackening can be very enlightening regarding the strong points of the proposed model. An important aspect to take into account is that the stiffness of the catenary depends on the actual contact force, mainly when the dropper slackening appear. At this point a nonlinear dependency of catenary stiffness with contact force appear. Hence, it is really important to provide a contact model to accurately compute the contact force, because when certain levels of contact force have been reached, catenary stiffness is no longer independent of the contact force. Thus, coupling catenary stiffness dependence on contact force with contact modelling ensure that nonlinear behaviour is accurately described.

Acknowledgements

This work has been partially supported by the Spanish Ministerio de Fomento under the project "*Optimización Electromecánica de Catenarias de Trenes de Alta Velocidad*" (Electromechanic Optimization of High Speed Trains). This support is gratefully acknowledged.

References

[1] G. Poetsch, J. Evans, R. Meisinger, W. Kortüm, W. Baldauf, A. Veitl, J. Wallaschek, Pantograph/catenary dynamics and control, *Vehicle System Dynamics* 28 (1997) 159–195.

[2] A.A. Shabana, J.R. Sany, A survey of rail vehicle track simulations and flexible multibody dynamics, *Nonlinear Dynamics* 26 (2001) 179–210.

[3] A. Collina, S. Bruni, Numerical simulation of pantograph-overhead equipment interaction, *Vehicle System Dynamics* 38 (4) (2002) 261–291.

[4] J.-H. Seo, H. Sugiyama, A.A. Shabana, Three-dimensional large deformation analysis of multibody pantograph/catenary systems, *Nonlinear Dynamics* 42 (2005) 199–215.

[5] M. Arnold, B. Simeon, Pantograph and catenary dynamics: a benchmark problem and its numerical solution, *Applied Numerical Mathematics* 34 (4) (2000) 345–362.

[6] M. Arnold, A pre-conditioned method for the dynamical simulation of coupled mechanical multibody systems, *Zeitschrift Fur Angewandte Mathematik und Mechanik* 8 (Suppl. 3) (2000) 817–818.

[7] B. Simeon, M. Arnold, Coupling DAE's and PDE's for simulating the interaction of pantograph and catenary, *Mathematical and Computer Modelling of Dynamic Systems* 6 (2000) 129–144.

[8] K. Manabe, Y. Fujii, Overhead system resonance with multi-pantograph and countermeasures, *Technical Report* 30, Quarterly Report of RTRI, 1989.

[9] K. Manabe, Periodical dynamic stabilities of a catenary–pantograph system, *Technical Report* 35, Quarterly Report of RTRI, 1994.

[10] T. Wu, M. Brennan, Basic analytical study of pantograph–catenary system dynamics, *Vehicle System Dynamics* 30 (1998) 443–456.

[11] Y. Guan, T.C. Lim, Comments on the stability analysis of pantograph–catenary system dynamics, *Journal of Sound and Vibration* 247 (3) (2001) 527–535.

[12] T. Wu, M. Brennan, Dynamic stiffness of a railway overhead wire system and its effect on pantograph–catenary system dynamics, *Journal of Sound and Vibration* 219 (3) (1999) 483–502.

[13] T. Park, C. Han, J. Jang, Dynamic sensitivity analysis for the pantograph of a high-speed rail vehicle, *Journal of Sound and Vibration* 266 (2) (2003) 235–260.

[14] A. Balestrino, O. Bruno, A. Landi, L. Sani, Innovative solutions for overhead catenary–pantograph system: wire actuated control and observed contact force, *Vehicle System Dynamics* 33 (2000) 69–89.

[15] O. Lopez-Garcia, A. Carnicero, V. Torres, Computation of the initial equilibrium of railway overheads based on the catenary equations, *Engineering Structures* 28 (10) (2006) 1387–1394.